Zheng J
Cardiff University
School of Engineering

Bhaduri D
Cardiff University
School of Engineering

Brousseau E
Cardiff University
School of Engineering

FUTURE ENGINEERING

Modelling of Temperature Distribution in Orthogonal Machining

Heat generation during machining has a profound effect on the performance of cutting tools, tool life, machinability of materials, and workpiece surface integrity. Thus, measurement and monitoring of cutting temperature is necessary for tool condition monitoring as well as to achieve the targeted surface and mechanical integrity of the produced parts. However, experimental measurement of cutting temperature could often be challenging, time consuming and cost intensive, and hence prediction of temperature distribution at the machining zone via modelling is imperative. This study verifies and validates prior analytical models from the literature to generate the temperature distribution patterns within the cutting tool, chip, and workpiece during macro-machining. The temperature fields at the shear zone (chip-workpiece interface) and at the friction zone (chip-tool interface) are generated using MATLAB software. The data closely matches with the range of cutting zone temperature found in the literature, with only ~6-7% deviation.

Keywords:
Machining, orthogonal, temperature, shear, friction, modelling.

Corresponding author:
ZhenJ24@cardiff.ac.uk

J. Zheng, D. Bhaduri, and E. Brousseau, 'Modelling of Temperature Distribution in Orthogonal Machining', *Proceedings of the Cardiff University School of Engineering Research Conference 2024*, Cardiff, UK, 2024, pp. 52-56.

doi.org/10.18573/conf3.m

Nomenclature

a	thermal diffusivity, m^2/s.
B	fraction of the shear plane heat source conducted into the work material.
$(1-B)$	fraction of the shear plane heat source conducted into the chip.
c	Specific heat, J/g °C.
l_i	location of the differential small segment of the shear band heat source d relative to the upper end of it and along its width, m.
L	width of the shear band heat source, m.
q_{pl}	heat liberation intensity of a moving plane heat source, J/ms.
q_{pli}	heat liberation intensity of an induced plane heat source, J/ms.
q_{pls}	heat liberation rate of the shear plane heat source, J/ms.
R	distance between the moving line heat source and point M, where the temperature rise is concerned, m.
r	chip thickness ratio (= t_c / t_{chip} or V_{ch} / V_c).
t_c	depth of cut, or undeformed chip thickness, m.
w	width of cut, m.
X, z	the coordinates of the point where the temperature rise is concerned in the moving coordinate system, m.
Θ_M	temperature rise at point M, °C.
C, m, k	variable parameters, the range of C 2-2.2, the range of m 0.22-0.26, k=16.
φ	oblique angle, degree.
α	rake angle, degree.

INTRODUCTION

Since the development of the theoretical models of metal cutting back in the 1940's, assessment of heat generation and the consequent temperature distribution patterns at the machining zone has received considerable attention from the research community. Experimental techniques for measuring the total temperature at the machining zone have been developed over decades. These methods typically involve use of bi-metallic thermocouples or utilising the tool-workpiece combination as a thermocouple. However, experimental measurement of cutting temperature could often be challenging, time consuming and cost intensive. Thus, prediction of cutting temperature has been attempted via analytical and finite element-based modelling. The advent of computer technology has led to the increasing use of theoretical analysis methods, which are faster, time saving, and can predict fairly accurate and reliable temperature data during machining.

In orthogonal machining, heat is generated in three areas: at the primary shear zone between workpiece and chip; at the secondary friction zone between chip and cutting tool, and at the tertiary friction zone between cutting tool and workpiece. To simplify the modelling process, Komanduri and Hou [1-3]first introduced by Hahn (Proceedings of First U.S. National Congress of Applied Mechanics 1951. p. 661–6 only considered the heat source at the first two zones and ignored the friction heat between the tool and the workpiece. Hahn [4] developed a thermal model by considering a moving heat source. The study analysed the effect of different shear angles on the average temperature at the shear zone and the model showed good agreement with experimental data. Jaeger [5] also considered moving heat sources to predict temperature. A study was conducted to classify heat sources as either moving or stationary. When dealing with a heat source in motion, the temperature inside the material undergoes constant change, resulting in a dynamic temperature field. Hahn's model [4] was modified by Trigger and Chao [6], who applied it to an infinite plane. They used this theoretical model to calculate the temperatures at the shear and friction zones and compared them with the measured experimental data. The theoretical results showed a 15% increase in temperature compared to the experimental results, which was considered as a reasonable margin of error. This demonstrates that modifying parameters using this method can result in more precise temperature prediction models. In orthogonal machining, Hahn's model was modified by Komanduri and Hou [1-3] to create the temperature distribution patterns at the chip and workpiece interface, caused by the shear zone heat source. Similarly, Jaeger's model [5] was adapted to produce models of chip and tool temperatures influenced by the secondary friction zone heat source. Integrating the models provides a temperature distribution model when heat sources act at the shear and friction zones simultaneously. By incorporating Trigger and Chao's model [6], a complete temperature distribution model for the workpiece, chip, and tool can be obtained. However, this temperature prediction model for machining is only valid at the macro scale. When the temperature prediction model is applied in a micro-machining scenario, the effects of rubbing and ploughing, together with shear, will need to be taken into account. This paper presents a verification and validation of the prior work on analytical temperature modelling, by using MATLAB software which was not used in the previous studies.

MATERIALS AND METHODS

Materials

Detailed machining parameters are shown in Tables 1 and 2. In particular, Table 1 was used to calculate the temperature distribution in the chip and workpiece due to the shear plane heat source only. In this case, the dimension of the workpiece was 300 µm x 150 µm. The data in Table 2 were employed to calculate the temperature distribution in the chip, tool, and workpiece considering both the frictional heat source and the shear plane heat source. For this, the dimension of the workpiece was 2000 µm x 500 µm.

Work material	SAE B1113 steel
Tool	K2S carbide 20° rake, 5° clearance angle
Type of cut	Orthogonal
Cutting speed	V_c = 2.32 m/s
Undeformed chip thickness	t = 0.00006 m
Width of cut	w = 0.00384 m
Chip contact length	L_c = 0.0023 m
Cutting force	F_c = 356 N
Feed force	F_t = 125 N
Chip thickness ratio	r = 0.51
Thermal diffusivity	a = 0.00001484 m^2/s
Thermal conductivity	λ = 56.7 W/mK

Table 1. Cutting data from Loewen and Shaw [7].

Work material	Steel NE 9445
Tool	Triple carbide, rake angle α = 4°
Type of cut	Orthogonal
Cutting speed	V_c = 1.524 m/s
Depth of cut	t_c = 0.0002484 m
Width of cut	w = 0.002591 m
Length of tool-chip contact	L = 0.001209 m
Cutting force	F_c = 1681.3 N
Feed force	= 854.0 N
Chip thickness ratio	F_t = 0.375
Thermal properties	
Work material: NE 9445 steel	λ = 38.88 w/mK a = 0.000008234 m^2/s
Tool: carbide	λ_{tool} = 41.9w/mK a_{tool} = 0.0000104 m^2/s

Table 2. Cutting data from Trigger and Chao [6].

Methods

This work primarily replicates the temperature model developed by Komanduri and Hou [1-3], although by using MATLAB R2023a software, whereas [1-3] utilised an unspecified computer program. The materials listed in Tables 1 and 2 were also used in [1-3]. Komanduri and Hou [1-3] determined the temperature distributions resulted by the shear and friction plane heat sources and then combined them together to calculate the total temperature rise during orthogonal machining. The heat from the shear plane is transferred to the workpiece and chip, and the temperature rise at any point in the workpiece and chip can be determined by Eq. 1 and 2. At the same time, the temperature distribution at any point in the tool is calculated by Eq. 3.

When considering the frictional heat source, the temperature rise at any point in the chip can be calculated by Eq. 4, 5 and 6, while the temperature rise at any point in the tool is governed by Eq. 7, 8 and 9. Five temperature distribution curves were derived for the chip, workpiece, and tool. The tool and chip temperatures were then superimposed to produce the final temperature profile. Equations 5, 6 and 10 can be used to calculate the temperature of the chip when both the shear plane heat source and the friction plane heat source are considered. Equations 8 - 12 can be used to calculate the temperature of the tool. Equation 1 can be used to calculate the temperature of the workpiece.

(1)
$$\theta_{M_{workpiece}} = \frac{q_{pl}}{2\pi\lambda}\int_{l_i=0}^{L} e^{-\frac{(X-l_i\sin\varphi)V}{2a}} \begin{Bmatrix} K_0\left[\frac{V}{2a}\sqrt{(X-l_i\sin\varphi)^2+(z-l_i\cos\varphi)^2}\right] \\ +K_0\left[\frac{V}{2a}\sqrt{(X-l_i\sin\varphi)^2+(z+l_i\cos\varphi)^2}\right] \end{Bmatrix} dl_i$$

(2)
$$\theta_{M_{chip}} = \frac{q_{pls}}{2\pi\lambda}\int_{w_i=0}^{t_{ch}/\cos(\phi-\alpha)} e^{-(X-X_i)V/2a} \begin{Bmatrix} K_0\left[\frac{V}{2a}\sqrt{(X-X_i)^2+(z-z_i)^2}\right] \\ +K_0\left[\frac{V}{2a}\sqrt{(X-X_i)^2+(2t_{ch}-z-z_i)^2}\right] \end{Bmatrix} dw_i$$

(3)
$$\theta_{M\_tool} = \frac{q_{pli}}{2\pi\lambda_{tool}} \begin{Bmatrix} (B_{ind}+\Delta B_i)\int_{y_i=-b_0}^{+b_0} dy_i \int_{x_i=0}^{L}\left(\frac{1}{R_i}+\frac{1}{R_i'}\right)dx_i \\ -2\Delta B_i\int_{y_i=-b_0}^{+b_0} dy_i \int_{x_i=0}^{L}\left(\frac{x_i}{L}\right)^m\left(\frac{1}{R_i}+\frac{1}{R_i'}\right)dx_i \\ -C_i\Delta B_i\int_{y_i=-b_0}^{+b_0} dy_i \int_{x_i=0}^{L}\left(\frac{x_i}{L}\right)^k\left(\frac{1}{R_i}+\frac{1}{R_i'}\right)dx_i \end{Bmatrix}$$

(4)
$$\begin{aligned}\theta_{M\_chip} = \frac{q_{pl}}{\pi\lambda}\Big\{&(B_{chip}-\Delta B)\int_{l_i=0}^{L} e^{-(X-l_i)V/2a}[K_0(R_iv/2a)+K_0(R_i'v/2a)]dl_i \\ &+2\Delta B\int_{l_i=0}^{L}\left(\frac{l_i}{L}\right)^m e^{-(X-l_i)v/2a}[K_0(R_iv/2a)+K_0(R_i'v/2a)]dl_i \\ &+C\Delta B\int_{l_i=0}^{L}\left(\frac{l_i}{L}\right)^k e^{-(X-l_i)v/2a}[K_0(R_iv/2a)+K_0(R_i'v/2a)]dl_i\Big\}\end{aligned}$$

(5) $$R_i = \sqrt{(X-l_i)^2+z^2}$$

(6) $$R_i' = \sqrt{(X-l_i)^2+(2t_{ch}-z)^2}$$

(7)
$$\theta_{M\_tool} = \frac{q_{pl}}{2\pi\lambda} \begin{Bmatrix} (B_{tool}+\Delta B)\int_{y_i=-b_0}^{+b_0} dy_i \int_{x_i=0}^{L}\left(\frac{1}{R_i}+\frac{1}{R_i'}\right)dx_i \\ -2\Delta B\int_{y_i=-b_0}^{+b_0} dy_i \int_{x_i=0}^{L}\left(\frac{x_i}{L}\right)^m\left(\frac{1}{R_i}+\frac{1}{R_i'}\right)dx_i \\ -C\Delta B\int_{y_i=-b_0}^{+b_0} dy_i \int_{x_i=0}^{L}\left(\frac{x_i}{L}\right)^k\left(\frac{1}{R_i}+\frac{1}{R_i'}\right)dx_i \end{Bmatrix}$$

(8) $$R_i = \sqrt{(x-x_i)^2+(y-y_i)^2+z^2}$$

(9) $$R_i = \sqrt{(x-2L+x_i)^2+(y-y_i)^2+z^2}$$

(10)
$$\begin{aligned}\theta_{M\_chip} = \frac{q_{pl}}{\pi\lambda}\Big\{&(B_{chip}-\Delta B)\int_{l_i=0}^{L} e^{-(X-l_i)v/2a}[K_0(R_iv/2a)+K_0(R_i'v/2a)]dl_i \\ &+2\Delta B\int_{l_i=0}^{L}\left(\frac{l_i}{L}\right)^m e^{-(X-l_i)v/2a}[K_0(R_iv/2a)+K_0(R_i'v/2a)]dl_i \\ &+C\Delta B\int_{l_i=0}^{L}\left(\frac{l_i}{L}\right)^k e^{-(X-l_i)v/2a}[K_0(R_iv/2a)+K_0(R_i'v/2a)]dl_i\Big\} \\ &+\frac{q_{pls}}{2\pi\lambda}\int_{w_i=0}^{t_{ch}/\cos(\phi-\alpha)} e^{-(X-X_i)V/2a} \begin{Bmatrix} K_0\left[\frac{V}{2a}\sqrt{(X-X_i)^2+(z-z_i)^2}\right]+ \\ K_0\left[\frac{V}{2a}\sqrt{(X-X_i)^2+(2t_{ch}-z-z_i)^2}\right] \end{Bmatrix} dw_i\end{aligned}$$

(11)

$$\theta_{M\_tool} = \frac{q_{pl}}{2\pi\lambda}\begin{Bmatrix} (B_{tool}+\Delta B)\int_{y_i=-b_0}^{+b_0} dy_i \int_{x_i=0}^{L}\left(\frac{1}{R_i}+\frac{1}{R_i'}\right)dx_i - \\ 2\Delta B\int_{y_i=-b_0}^{+b_0} dy_i \int_{x_i=0}^{L}\left(\frac{x_i}{L}\right)^m\left(\frac{1}{R_i}+\frac{1}{R_i'}\right)dx_i \\ -C\Delta B\int_{y_i=-b_0}^{+b_0} dy_i \int_{x_i=0}^{L}\left(\frac{x_i}{L}\right)^k\left(\frac{1}{R_i}+\frac{1}{R_i'}\right)dx_i \end{Bmatrix} + \frac{q_{pli}}{2\pi\lambda_{tool}}\begin{Bmatrix} (B_{ind}+\Delta B_i)\int_{y_i=-b_0}^{+b_0} dy_i \int_{x_i=0}^{L}\left(\frac{1}{R_i}+\frac{1}{R_i'}\right)dx_i \\ -2\Delta B_i\int_{y_i=-b_0}^{+b_0} dy_i \int_{x_i=0}^{L}\left(\frac{x_i}{L}\right)^m\left(\frac{1}{R_i}+\frac{1}{R_i'}\right)dx_i \\ -C_i\Delta B_i\int_{y_i=-b_0}^{+b_0} dy_i \int_{x_i=0}^{L}\left(\frac{x_i}{L}\right)^k\left(\frac{1}{R_i}+\frac{1}{R_i'}\right)dx_i \end{Bmatrix}$$

(12) $x_i = l_i$

RESULTS AND DISCUSSION

The MATLAB reproduction of the temperature distribution data across the tool, workpiece and chip is shown in Figs. 1 and 2. The temperature values are largely consistent with that of Komanduri and Hou's model [1-3], although some discrepancies were noted.

Figure 1 shows the temperature distribution generated by shear plane heat source between the chip and workpiece. The temperature of the workpiece at the shear plane is ~120°C, whereas the maximum temperature of the chip is 280°C. In contrast, the temperature is lower (only ~140°C) when closer to the chip-tool interface region. In the workpiece, the temperature is ~20°C higher than that of [1-3], at the equivalent locations. Figure 2 shows the average temperature distributions in the workpiece, chip, and tool. Difference in the materials' properties cause temperature variations at the contact surfaces. The maximum temperature at the chip-tool contact surface is 700°C, which decreases as the distance from the contact surface increases. The maximum temperature of the workpiece in the middle of the shear plane reaches up to ~250°C. The maximum temperature at the chip-workpiece contact surface, within the chip was ~420-430°C, which was marginally higher than that reported in [1-3].

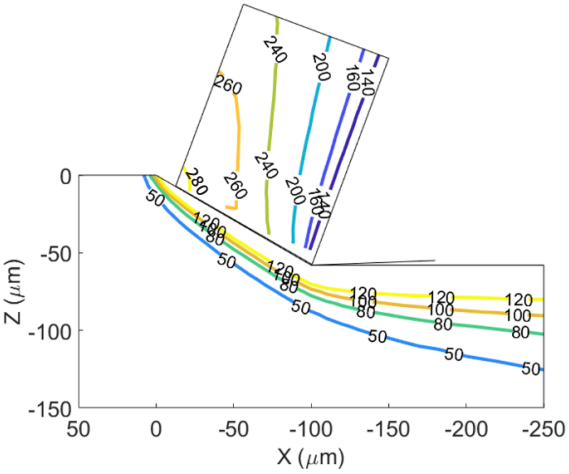

Fig. 1. Temperature distribution in the chip and workpiece due to the shear plane heat source.

The temperature plots using MATLAB did not produce smooth curves within the chips, nearer the shear plane. This was possibly because fewer points were generated by the matrix when calculating the temperature values. Nonetheless, the temperature distribution data was roughly in agreement with [1-3], with ~6-7% variation. Using the MATLAB2023 version, the first temperature model in Fig. 1 was obtained in 5 minutes, while the second model in Fig. 2 was calculated in 14 minutes. Currently, the program's running time is considerably lengthy. As more parameters and complexities will be added in subsequent temperature modelling for micro and nanomachining scenarios, modifications are necessary to shorten the program's running time and to increase its efficiency.

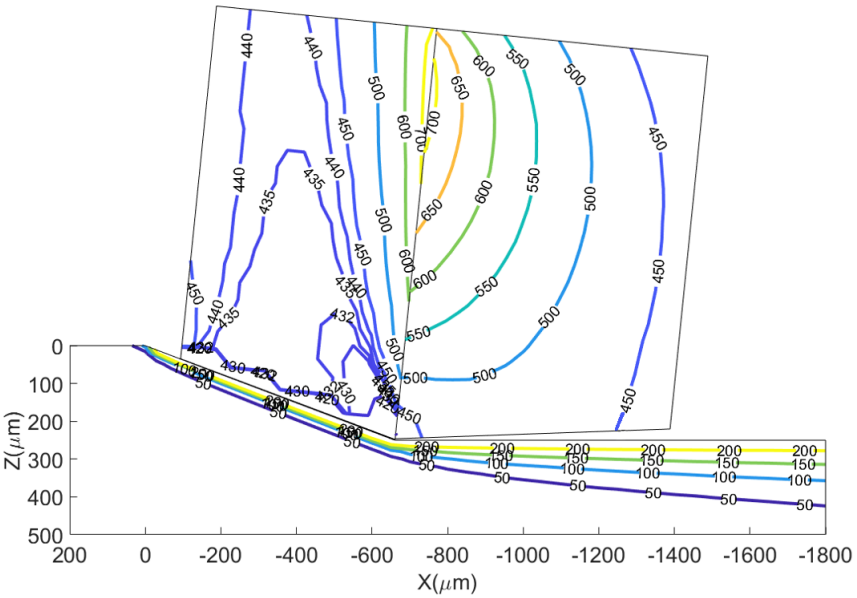

Fig. 2. Temperature distribution in the chip, tool, and workpiece considering both the frictional heat source and the shear plane heat source. Material: Steel NE 9445.

CONCLUSIONS

The temperature distribution data resulted from the shear plane and friction plane heat sources matches well with the prior analytical models. Thus, it is feasible to use MATLAB programs to adopt the model for predicting machining temperatures at a macroscopic level. Future work will focus on modifying these models to predict temperatures during micro and nanomachining. This will require encompassing the effects of rubbing and ploughing as material failure modes, together with the conventional shear failure mechanism.

Acknowledgments
The authors acknowledge the funding support received from China Scholarship Council.

Conflicts of Interest
The authors declare no conflict of interest.

REFERENCES

1. R. Komanduri and Z. B. Hou, 'Thermal modeling of the metal cutting process', *International Journal of Mechanical Sciences*, vol. 42, no. 9, pp. 1715–1752, Sep. 2000. doi.org/10.1016/S0020-7403(99)00070-3

2. R. Komanduri and Z. B. Hou, 'Thermal modeling of the metal cutting process — Part II: temperature rise distribution due to frictional heat source at the tool–chip interface', *International Journal of Mechanical Sciences*, vol. 43, no. 1, pp. 57–88, Jan. 2001. doi.org/10.1016/S0020-7403(99)00104-6

3. R. Komanduri and Z. B. Hou, 'Thermal modeling of the metal cutting process — Part III: temperature rise distribution due to the combined effects of shear plane heat source and the tool–chip interface frictional heat source', *International Journal of Mechanical Sciences*, vol. 43, no. 1, pp. 89–107, Jan. 2001. doi.org/10.1016/S0020-7403(99)00105-8

4. R.S. Hahn, 'On the temperature developed at the shear plane in the metalcutting process', *Journal of Applied Mechanics-Transactions of the ASME*. vol. 18. no. 3, pp.323-323, 1951.

5. J. C. Jaeger, 'Moving sources of heat and the temperature at sliding contacts', *Journal and Proceedings of the Royal Society of New South Wales*, vol. 76, no. 3, pp. 203-224, May 1943. doi.org/10.5962/p.360338

6. K. J. Trigger and B. T. Chao, 'An Analytical Evaluation of Metal-Cutting Temperatures', *Journal of Fluids Engineering*, vol. 73, no. 1, pp. 57–66, Jan. 1951. doi.org/10.1115/1.4016141

7. E. G. Loewen and M. C. Shaw, 'On the Analysis of Cutting-Tool Temperatures', *Journal of Fluids Engineering*, vol. 76, no. 2, pp. 217–225, Feb. 1954. doi.org/10.1115/1.4014799

Cynhadledd Ymchwil Peirianneg Caerdydd
Cardiff Engineering Research Conference

E. Spezi and M. Bray (eds.) 2024. *Proceedings of the Cardiff University School of Engineering Research Conference 2024.* Cardiff: Cardiff University Press.
doi.org/10.18573/conf3

Cardiff University School of Engineering Research Conference 2024 was held from 12 to 14 June 2024 at Cardiff University.

The work presented in these proceedings has been peer reviewed and approved by the conference organisers and associated scientific committee to ensure high academic standards have been met.

Cardiff University Press | Gwasg Prifysgol Caerdydd

First published 2024

Cardiff University Press
Cardiff University, Trevithick Library
First Floor, Trevithick Building, Newport Road
Cardiff CF24 3AA

cardiffuniversitypress.org

Editorial design and layout by
Academic Visual Communication

ISBN: 978-1-9116-5351-6 (PDF)